MICHIGAN STATE UNIVERSITY

CYCLOTRON LABORATORY

OBSERVATION OF M1 STRENGTH IN ZIRCONIUM ISOTOPES BY PROTON INELASTIC SCATTERING

G.M. CRAWLEY, N. ANANTARAMAN, A. GALONSKY, C. DJALALI, N. MARTY, M. MORLET, A. WILLIS, J.-C. JOURDAIN and P. KITCHING

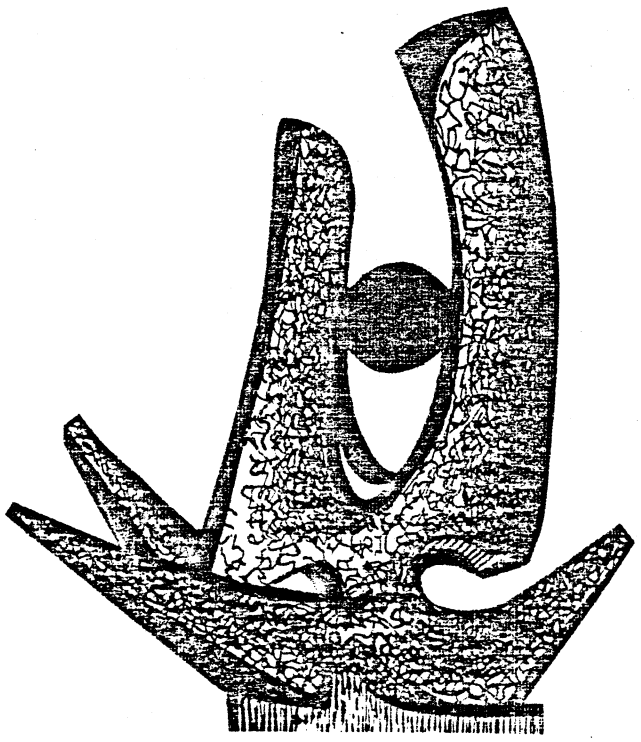

FEBRUARY 1982

MSUCL-368

MSUCL-368
February 1982

Observation of M1 strength in zirconium isotopes by proton inelastic scattering

G.M. Crawley, N. Anantaraman and A. Galonsky

National Superconducting Cyclotron Laboratory
Michigan State University
East Lansing, Michigan 48824, USA

and

C. Djalali, N. Marty, M. Morlet, A. Willis, J.-C. Jourdain and P. Kitching*

Institut de Physique Nucléaire
F-91406
Orsay, France

Abstract

A broad resonance has been observed by inelastic scattering of 200 MeV protons from ^{90}Zr, ^{92}Zr, ^{94}Zr and ^{96}Zr. This resonance has a sharply forward peaked angular distribution and an excitation energy and strength which strongly suggest that it is the M1 giant resonance. Microscopic distorted wave impulse approximation calculations match the shape of the angular distribution reasonably well. The strength, however, is only about 30% of that predicted.

I. INTRODUCTION

The study of M1 states in nuclei allows the exploration of the nuclear spin degrees of freedom, which is interesting for a number of reasons[1]. The shell model predicts that there should be M1 states (1^+ in even-even nuclei) made when the spin of a particle in a j-unsaturated shell is flipped, i.e., $j=l+1/2 \rightarrow j=l-1/2$. The M1 strength is therefore a measure of the extent to which unsaturated spin-orbit-partner orbits are occupied in the nuclear ground state. Secondly, the M1 strength gives a check on the renormalization (due to core polarization and mesonic effects) of the magnetic charge (effective g-factors).[2] This renormalization, until now, has been determined mainly from the study of magnetic moments. Thirdly, in scattering experiments the M1 strength allows, in principle, the determination of the spin-dependent components of the effective interaction between the nucleons in the projectile and the target. At small angles and at bombarding energies above 100 MeV/nucleon, where the $V_{\sigma\tau}$ component is dominant[3,4], the strength should be particularly sensitive to this one component. Finally, since the one pion exchange potential involves spin and isospin transfer of one, and since the $V_{\sigma\tau}$ operator involves spin flip and isospin flip, the magnitude of this operator at large momentum transfers is important in determining the pionic interactions with nuclei and in particular whether or not a phase transition to a pion condensed phase can take place[5,6].

Various shell model estimates give little variation in the predicted excitation energy of the M1 state[1,7], but searches to locate it in targets having $A \geq 60$ using both inelastic electron[8,9] and inelastic proton[10,11] scattering have, until recently, proven unsuccessful. Recent observations[12-14], in intermediate-energy (p,n) reactions on a number of targets, of a broad peak which has been identified as the giant Gamow-Teller (GT) state (in which $J^{\pi} = 1^{+}$) have provided a clue for the search for the M1 transition in the parent nucleus. The fact that the GT state was more prominent at $E_p \geq 120$ MeV than at 45 MeV[15] implied that the $V_{\sigma\tau}$ component of the effective interaction had increased relative to the other components, as is also suggested by the energy dependence of the nucleon-nucleon interaction[4]. This implies that the 1^{+}, M1 state, which is excited by means of this same component of the effective interaction, might also be more strongly excited at higher bombarding energies. Since the orbital angular momentum transfers involved in this $0^{+} \rightarrow 1^{+}$ transition are zero and two, the cross section for the state should be peaked at 0^{o} and fall off rapidly with angle. These considerations suggested a search for the M1 transition using inelastic scattering of high energy (E>100 MeV) protons at forward angles.

In our first measurement, carried out using the 201 MeV proton beam from the Orsay synchrocyclotron, a broad peak was seen in three even-even zirconium isotopes. In a preliminary report of this work[16], the peak was suggested

to correspond to the giant M1 transition. A similar feature has been observed in ^{90}Zr at TRIUMF[17]. We have since extended the search[18] and located a concentration of M1 strength in fifteen other medium weight nuclei ranging from ^{40}Ca to ^{140}Ce. These observations have also sparked considerable theoretical interest in the problem of M1 transitions[19,20].

The present paper presents a more complete description of the work on the zirconium isotopes including data on the additional isotope ^{96}Zr. Comparisons are made with (p,n) and (e,e') results[14,21] and with a microscopic distorted wave analysis.

II. EXPERIMENTAL ARRANGEMENT

The data were taken at the Orsay synchrocyclotron with a large magnetic spectrometer and a computerized detection system[22,23]. The experiment was done at the smallest possible angles so that the L=0 transfers associated with $0^{+} \rightarrow 1^{+}$ transitions would be enhanced above other L transfers. The detection system used was one designed especially to work at very forward angles. A more complete description of the experimental setup is contained in two forthcoming papers[24,18]. The key feature of the system was that the trajectory of a particle could be reconstructed from its positions in two proportional counters. Particles with trajectories outside a certain angular range ($\pm 0.5^{o}$ in the present experiment) were rejected.

The differential efficiency of the detectors was not completely uniform. Instead some spurious sharp peaks both positive and negative, were observed. Two different approaches were taken to alleviate this problem. First, each spectrum was taken twice with slightly different spectrometer fields to identify spurious structure. The Zr spectra displayed are the sum of these two different runs and are thus averages over the microstructure. Secondly, the actual response of the detectors was determined by measuring the scattering from ^{208}Pb in the region around 100 MeV excitation energy. From work with germanium detectors this region is known to be quite flat[25]. The M1 resonance region was positioned on parts of the two detectors which had no large defects. The ^{208}Pb spectra were measured before and after the data runs and the detector response was found to be very stable over this 5 day period. The ^{96}Zr spectra were corrected for the detector response before analysis. Most of the remaining spectra were taken when the differential nonlinearities were less severe and did not require correction. The intensity of the beam was kept low enough so that the overall counting rate was less than 500/sec. At 4^{o} this was about 100 nA. As seen on an alumina scintillator, the size of the beam at the target was about 6 to 8 mm diameter.

The targets used were calcium (natural Ca; 15.0 mg/cm^2), ^{90}Zr (98% enriched; 10.2 and 18.9 mg/cm^2), ^{92}Zr (95% enriched; 25.4 mg/cm^2), ^{94}Zr (99% enriched; 16.4 mg/cm^2) and ^{96}Zr

(57% enriched, with 4%, ^{94}Zr, 27% ^{92}Zr, 2% ^{91}Zr and 10% ^{90}Zr; 5.4 mg/cm^2). The energy resolution obtained was about 80 keV FWHM. Calcium was used so that we could empirically determine a 1$^+$ angular distribution by exciting the known[26] 1$^+$ state in ^{40}Ca at 10.31 MeV.

The spectra were energy calibrated by recording the position of the elastic peak for various magnetic field settings and by using the positions of known low-lying states of ^{90}Zr, ^{40}Ca and ^{12}C. The calibration is good to about $\pm$20 keV.

Absolute values of the cross sections were determined by comparison with the known p-p scattering cross sections using a polyethylene target. In fact, when cross sections were computed in the standard manner from the target thickness, the solid angle of the spectrometer, a presumed 100% detection efficiency (except for small dead time corrections), and the quantity of charge collected, the result was the same as that from the p-p scattering comparison to within 5%. A further check on absolute values is afforded by noting that elastic scattering cross sections measured on ^{90}Zr at angles out to 18^{o} were, on the average, only 5% below those computed from the optical model parameters of Schwandt et al[27]. The normalization is thus well established.

III. RESULTS

Spectra of protons scattered from Ca at laboratory angles of 3^{o} and 7^{o} are shown in Fig. 1. At 3^{o} the spectrum

shows only 4 peaks clearly--at excitation energies of 6.94(1^-), 8.43(2^-), 10.31(1^+) and 12.03 MeV.

The L=0 angular distribution observed[16] for the 12.03 MeV state implies that its J^π is either 0^+ or 1^+; and since it was not seen in back-angle inelastic electron scattering[26], we had speculated in our previous paper[16] that it was probably a 0^+ state. However, a recent (p,n) measurement[28] on ^{40}Ca shows a state in ^{40}Sc at an excitation of 4.3 MeV, which could be the analog of the 12.03 MeV state in ^{40}Ca. If so, it would have T=1 and would probably not be a 0^+ state since the V_τ operator is much weaker than the $V_{\sigma\tau}$ operator. This would also suggest that the J^π of the 12.03 MeV state in ^{40}Ca is probably 1^+. The fact that this state is not seen in forward angle inelastic alpha[29] and inelastic deuteron[22] scattering also implies that it is not a 0^+ state. The nature of the 12.03 MeV state obviously needs further clarification.

In the 7^o spectrum many peaks are observed and the states populated by L=0 are now much weaker. Contaminant peaks from the small amount of oxygen impurity on the target are shown shaded. The angular distributions for the 10.31, 12.03 and 8.43 MeV states were given in Ref. 16.

Spectra from the four even-even zirconium isotopes at a laboratory angle of 4^o are shown in Fig. 2. In all the isotopes a peak is observed which shows up clearly above

the background at an excitation energy between 8 and 9 MeV. The shape of the peak varies from isotope to isotope and is neither smooth nor symmetrical. In all cases, the peak area was extracted by first subtracting a background, shown for 4^o as the dashed line in Fig. 2. The peak limits were selected at a forward angle, where the peak is best defined, and the same limits of excitation energy were then used to determine the peak area at the other angles.

A large broad peak is also observed near 15 MeV excitation energy in each isotope. This is presumably a mixture of the giant dipole, quadrupole and monopole resonances[30] with the dipole strength dominanting in the 4^o spectra shown[31]. No evidence was found for fine structure within the broad peaks near 9 MeV, even though the overall energy resolution in the experiment was about 80 keV.

The excitation energy, full width at half maximum (FWHM) and the base width for each of the lower lying broad peaks is given in Table 1. The excitation energy of the peak shows a very slight decrease from ^{90}Zr to ^{96}Zr. While the FWHM also shows a small decrease from ^{90}Zr to ^{96}Zr, the energy region over which enhanced structure is observed is similar in all four isotopes as illustrated by the base width of the peak.

The observed excitation energy for the peak is consistent with that expected for an M1 state in ^{90}Zr. Various theoretical estimates predict that the excitation energy of the M1 state in ^{90}Zr should be about 9 MeV and a recent paper by Toki et al.[19] gives values for all even-even zirconium

isotopes which are in good agreement with those observed here.

An estimate of the excitation energy can also be made from the (p,n) results. In the ^{90}Zr(p,n) experiment at 120 MeV[12,32], there is evidence for a small peak on the high excitation energy side of the main GT peak. This peak is presumably the T=5 component of the GT strength and is the analogue of the M1 state in ^{90}Zr also with T=5. Thus the difference in energy of the T=5 state and the 0^+ isobaric analogue state (IAS) in ^{90}Nb should correspond to the excitation energy of the M1 state in ^{90}Zr. The results[32] from the (p,n) reaction at 120 MeV on all the stable even-even zirconium isotopes are also given in Table 1 and are seen to be in reasonably good agreement with the excitation energies of the peaks observed in (p,p').

An earlier inelastic electron scattering measurement[33] on ^{90}Zr also showed a small bump near 9 MeV excitation energy. However, this measurement had some experimental difficulties and the work has not been published. A recent high resolution inelastic scattering experiment[21] claims to identify three 1^+ states in ^{90}Zr at 8.233, 9.000 and 9.371 MeV with seven other possible 1^+ states at 7.774, 7.868, 8.142, 8.366, 8.602, 9.439 and 9.520 MeV, although the dominant strength observed in this region is M2. While the differential non linearities in the (p,p') counter make it difficult to identify small sharp structures unambiguously, there is no evidence in the (p,p') spectra for sharp peaks corresponding to those observed in (e,e'). In particular the peak at 9.000 MeV

observed in (e,e')is separated by more than 300 keV from any neighboring 1^+ state yet we see no evidence for its excitation in the present experiment. The upper limit for the summed strength given by the (e,e') results is 16% or 25% of the total RPA M1 strength calculated in a separable interaction model using bare and effective g-factors, respectively. These limits will be compared with the present results later in the paper.

The cross sections for the broad features centered between 8 and 9 MeV observed in (p,p') show a very rapid decrease with angle. This is seen clearly in Fig. 3 where th spectra from ^{92}Zr(p,p') are shown at laboratory angles of 3^o and 7^o. Although the background from the tail of the elastic scattering peak has grown substantially at 3^o, even compared to the 4^o spectrum of Fig. 2, the peak at about 9 MeV excitation energy still stands out clearly. At 7^o, the low-lying states are much more clearly visible, the background is much lower, but the peak near 9 MeV is very much weaker.

The angular distributions of the broad peaks are shown in Fig. 4 together with theoretical calculations which will be discussed in the next section. All four angular distributions are similar in shape and fall off sharply with angle. The angular distribution for ^{90}Zr appears to fall somewhat more steeply than for the other isotopes. These angular distributions are also very similar to the angular distributions observed[16] for the known 1^+ state in ^{40}Ca at 10.3 MeV. The angular distribution for the ^{90}Zr(p,n) reaction measured

at 200 MeV[14] is shown as a dot-dashed line in Fig. 4. The shape of this angular distribution matches quite closely the measured shape of the ^{90}Zr(p,p') angular distribution at 201 MeV. The comparison of the strengths of these two reactions will be discussed in Section V.

The absolute magnitudes of the cross sections at the most forward angles measured are very similar for all four isotopes. However, the present measurement for ^{90}Zr at 4^{o} is lower than the value of 7.2±2.0 mb/sr measured by Bertrand et al.[17] for ^{90}Zr(p,p') at 200 MeV. An examination of their spectrum suggests that at least some of the difference may arise from the choice of background since the background shown in the work from TRIUMF is substantially lower than the data points on the high excitation side of the 9 MeV peak.

IV. MICROSCOPIC CALCULATIONS

Microscopic inelastic scattering calculations were performed in the distorted wave impulse approximation (DWIA) with a modified version of the code DWBA70[34], which includes knockon exchange contributions exactly. In the DWIA, the effective nucleon-nucleon (N-N) interaction is taken to be the free N-N t-matrix. In addition to this interaction, the other main inputs required in the calculation are the optical potential describing the scattering of the projectile from the Zr target and the amplitudes describing the transition

from the nuclear ground state to the final state. For the single-particle states involved in the transition, harmonic oscillator bound-state wave functions were used, with an oscillator constant obtained from $\hbar\omega = 41\ A^{-1/3}$ MeV. The results are not sensitive to the exact value of this parameter.

The interaction derived by Love and Franey[4] from 210 MeV two-nucleon scattering amplitudes was used for the effective interaction in the calculations. It consists of a sum of real and imaginary central, spin-orbit and tensor terms of various ranges.

For the p + Zr optical potential, two sets were used. Set I was obtained from a global energy- and target mass-dependent potential determined recently by Schwandt et al.[27] by combining extensive elastic differential cross sections at a number of energies extending up to 180 MeV with elastic analyzing power data in the same energy range; its parameters were evaluated for the case of 200-MeV protons incident on ^{90}Zr. This potential supercedes the fixed-spin-orbit potential of Nadasen et al.[35]. Potential Set II is one determined by searching on data obtained in a previous measurement of elastic scattering from ^{90}Zr from 4^{o} to 52^{o} [36] using the optical-model code JIB IV.[37] The two sets are listed in Table II, using the same notation as in Ref. 35.

Figure 5 shows the elastic scattering data from which potential Set II was determined. Also shown are the calculated angular distributions obtained using Set I (dashed

curve) and Set II (full curve). The Set I potential, determined by a global search on scattering data at energies below 200 MeV, gives a good fit to the data below about 24^{o} but the fit is much poorer at more backward angles. Moreover, as mentioned in Section II, the good fit (in both magnitude and shape) obtained with the Set I potential at forward angles implies that the absolute cross section detemination in the present measurement is free of substantial error.

The microscopic DWIA calculations also require transition amplitudes as input. These depend on the model used to calculate the structure of the ground and excited states. For the 1^{+} states in $^{90-94}Zr$, the shell-model calculations of Anantaraman and Wildenthal[20] were used to obtain the transition amplitudes. In those calculations, only neutron excitations were considered, and ^{80}Zr was treated as the core. The valence neutrons were distributed within the $1g_{9/2}$, $2d_{5/2}$, $3s_{1/2}$, $2d_{3/2}$ and $1g_{7/2}$ orbitals, subject to the restriction that the $g_{9/2}$ orbital was occupied by either 9 or 10 particles. In the case of ^{90}Zr, this model gave the configuration $(g_{7/2}\, g_{9/2}^{-1})1^{+}$ for the 1^{+} state, which is identical to that expected on the simplest shell model. In the case of $^{92,94}Zr$, the model includes all configurations which give rise to 1^{+} states. No shell model calculation was done for ^{96}Zr because of the large dimensionalities of the problem.

We turn now to the results of the DWIA calculations performed for the 1^{+} states. In the model of Ref. 20, the

1^{+} strength is concentrated in a single state in ^{90}Zr, whereas in ^{92}Zr and ^{94}Zr, appreciable strength is found in the lowest 20 and 50 states, respectively. Since DWBA calculations for all these separate states would be prohibitively time consuming and expensive, an alternative approach was used. A B(M1)↑ strength was calculated for each of these states.[20] Microscopic (p,p') calculations were done for a few of the states and it was observed that the (p,p') cross sections for transitions to them were in strict proportion to their B(M1)↑ strengths. The strongest state contained 51% of the total B(M1)↑ strength in the case of ^{92}Zr and 18% in the case of ^{94}Zr. The (p,p') cross sections calculated for these two states were therefore multiplied by factors of 1/0.51 and 1/0.18, respectively, to get the total 1^{+} cross sections in the two nuclei.

All the curves shown in Fig. 4 have been individually normalized to the data. The solid curves are the results of the microscopic calculations for the 1^{+} transitions in $^{90,92,94}Zr$ using the full 210-MeV Love-Franey (L-F) interaction. The two sets of optical potentials gave the same shapes for the angular distributions, with Set I giving about 10% larger cross section than Set II. (The cross sections obtained with the Nadasen optical potential evaluated at 200 MeV were about 60% larger than those with the later potential of Schwandt et al. (Set I). The main difference between them is that the strength of the volume imaginary term is 30% greater in Set I.)

The calculated 1^+ angular distribution shapes are nearly identical for $^{90,92,94}Zr$ in the angular range of interest, showing that the admixture of the $d_{3/2}d_{5/2}^{-1}$ component in the latter two cases has little effect on the shape. The differences in the experimental shapes are more pronounced. This leads to the result that the quality of the fit is good for ^{92}Zr and ^{94}Zr but poor for ^{90}Zr.

In the case of ^{96}Zr, the lack of transition amplitudes precluded microscopic calculations. In view of the fact (illustrated in Fig. 4) that the angular distributions calculated for the transition to the 1^+ states in $^{90,92,94}Zr$ are very similar despite the different $d_{3/2}d_{5/2}^{-1}$ admixtures present in them, we expect that the same shape would also be valid in the case of ^{96}Zr. In fact, when the angular distribution shape calculated for the ^{90}Zr transition is compared with the data for ^{96}Zr (as shown by the solid line) a good fit is obtained.

To improve the fit in the case of ^{90}Zr, various changes in the input parameters of the calculation were tried. Use of different optical potentials and modest changes in the oscillator constant did not alter the calculated shape.

A further DWIA calculation was also carried out using the code RESEDA[38] for the case of ^{90}Zr using the Set II optical model parameters and a simple ($g_{7/2}\ g_{9/2}^{-1}$) wave function. The details of the calculation are given in ref. 24. There, calculations are carried out for a number of low lying states in ^{208}Pb and good agreement is obtained with the measured cross sections. In the ^{90}Zr case, the

calculation is shown in Fig. 4 as a dashed line. For this calculation the normalization of theory to experiment for ^{90}Zr requires multiplication by a factor of 0.41.

The experimental and calculated cross sections at 4° for the 1^+ transitions in the Zr isotopes are listed in Table III, along with the factors N($=\sigma_{exp}/\sigma_{calc}$) used to normalize the calculated curves to the data. Optical potential Set II and the 210-MeV L-F interaction were used in three of the calculations from which these numbers were extracted. The other calculation for ^{90}Zr, using the code RESEDA, gives a normalization factor N of 0.41 and is also given in Table III. The two calculations give rather different normalizations for ^{90}Zr. While the RESEDA calculation gives a slightly better fit to the ^{90}Zr angular distribution than the DWBA70 calculation, the absolute value of the calculated cross section is probably less reliable. Exchange effects, which are known to be very significant in the calculations, are treated exactly in DWBA70 but are treated only approximately in RESEDA. The values of N determine the degree of enhancement or quenching of the experimental cross section relative to the theoretically expected one. For all four isotopes the experimental cross sections are the same within errors and the three calculated cross sections using DWBA70 are also equal. This means that we find about the same degree of quenching in all the isotopes.

We estimate the overall uncertainty in N by adding in quadrature the uncertainties of the measurement ($\pm$15%) and the uncertainties of the calculation, due to the optical potential ($\pm$15%) and the effective interaction ($\pm$20%).

Combining together both calculations for ^{90}Zr, gives an average 1^+ normalization factor of N = 0.3 ± 0.1, for all the isotopes. This is about the same amount of quenching as is observed in (p,n) reactions at intermediate energies to 1^+ states in medium and heavy nuclei[14]. A more detailed comparison between (p,p') and (p,n) reactions in the case of ^{90}Zr is given in the next section.

V. COMPARISON BETWEEN (p,p') AND (p,n) STRENGTHS

In general, the (p,p') transition to the M1 state can proceed through the V_σ and $V_{\sigma\tau}$ parts of the central interaction, while the transition to the analogue of this state in a (p,n) reaction is mediated by the $V_{\sigma\tau}$ part alone. There will also be contributions to both transitions from the tensor and spin-orbit forces, but these are expected to be small at small momentum transfer, corresponding to very forward angles. In addition, the V_σ term is expected to be about one sixth of $V_{\sigma\tau}$ at a bombarding energy of 200 MeV, according to the calculations of Love and Franey[4]. Thus initially we may assume that the (p,p') reaction to the 1^+ state and the (p,n) reaction to its analogue are mediated by the same piece of the effective interaction, namely the $V_{\sigma\tau}$ piece. With this assumption, it is possible to simply relate the cross section for (p,n) to the T=5 1^+ state in ^{90}Nb to the cross section for exciting the M1 transition in ^{90}Zr by (p,p').

If one assumes that ^{90}Zr has closed proton and neutron shells, then for one-step processes acting on neutrons only and mediated by $V_{\sigma\tau}$, the (p,p') cross section to the M1 state is related to the (p,n) cross section for exciting

the $T_>$ component of the GT resonance by the equation

$$\sigma(p,p')\ (M1) = \frac{5}{2}\sigma(p,n)\ (T=5). \qquad (1)$$

With similar model assumptions, the ratio of the (p,n) cross sections for the T=4 and T=5 states should be 9:1. Therefore, if one compares the (p,p') cross section with the total (p,n) cross section to both T=4 and T=5 states in ^{90}Nb (since the T=4 and T=5 states are not always clearly resolved in the (p,n) reaction), we find

$$\sigma\ (p,p')\ (M1) = 0.25\sigma(p,n)\ \ (T=4+T=5) \qquad (2)$$

The measured value of the ^{90}Zr (p,n) cross section at a bombarding energy of 200 MeV to the T=4 and T=5 unresolved GT states is 50 ± 12 mb/sr.[14] This simple model would thus predict a (p,p') cross section for the M1 state at 0° to be 12.5 ± 3 mb/sr.

In order to make the comparison, it is necessary to extrapolate the (p,p') cross section to 0°. The two DWIA calculations for ^{90}Zr shown in Fig. 4, extrapolate to slightly different values at 0° but both values lie within the range 7.0 ± 0.8 mb/sr. An extrapolation using the empirical (p,n) angular distribution at 200 MeV, shown as a dot-dashed curve in Fig. 4, gives a value at 0° which also falls within this range.

This very simple theory can be refined in a number of ways. First, it is known tht the ratio of the cross sections for T=4 to T=5 states in (p,n) at 120 MeV, where they can be resolved, is not 9:1 but is closer to 13:1[32]. This is explained by Bertsch et al.[39] as arising from mixing

of the T=4 ($g_{7/2}g_{9/2}^{-1}$) state with a low lying 1^+, T=4 state with the configuration $g_{9/2}g_{9/2}^{-1}$. Thus, in comparing with (p,p'), the simple prediction given previously should be reduced by a factor of 10/14, as shown in Table IV. This makes the agreement somewhat closer.

Another effect which can be calculated is the contribution of the V_σ interaction to the (p,p') cross section. This contribution has been calculated using DWBA70 with the values of V_σ and $V_{\sigma\tau}$ taken from the L-F interaction at 210 MeV. Unlike the situation at lower bombarding energies, where there is a cancellation between V_σ and $V_{\sigma\tau}$ which reduces the overall cross section, the L-F interaction implies that the (p,p') cross section is increased by about 25% due to the isoscalar contribution. This effect tends to make the prediction disagree even more with the observed values, as shown in Table IV.

So far, the estimates have assumed that the distortion effects are the same for (p,p') and (p,n). A calculation of the distortion factors made in the usual manner by comparing DWBA70 calculations for plane waves with one for distorted waves for both (p,n) and (p,p') at 200 MeV suggests that the distortion effects are different in the two cases and tend to reduce the (p,p') cross sections by about 20% more than they reduce the (p,n) cross sections. The final comparisons at 0° (and also at 4° where no extrapolation is required) are displayed in Table IV. The ratio of actual to predicted cross sections at both angles is about 0.7.

VI. SUMMARY AND CONCLUSIONS

The inelastic scattering of 201-MeV protons from ^{90}Zr, ^{92}Zr, ^{94}Zr and ^{96}Zr shows a resonance at an excitation energy between 8 and 9 MeV with a FWHM of about 1.5 MeV. The angular distribution of this resonance is very forward peaked and is characteristic of an angular momentum transfer of zero. The shape of the angular distribution is very similar to that of the GT peak observed in the ^{90}Zr(p,n) reaction at 200 MeV. The excitation energy and angular momentum transfer suggests that this resonance is the giant M1 resonance, the analogue and anti-analogue of which have both been seen in (p,n) reactions on the zirconium isotopes. The strength of the resonance observed in (p,p') is about 70% of the strength one would predict from scaling the 200 MeV (p,n) cross section with a simple model of the nuclear wave functions. A microscopic distorted wave impulse approximation provides reasonably good agreement with the shape of the measured angular distribution. However, the strength observed is only about 30% of the calculated strength in ^{90}Zr, ^{92}Zr and ^{94}Zr.

ACKNOWLEDGEMENTS

This work was partly supported by the U.S. National Science Foundation under Grant No. PHY-78-22696. Two of the authors (GMC and NA) received travel support from the INT Division of the National Science Foundation. One of

the authors (GMC) would also like to thank the University of Paris XI for financial support and warm hospitality during his visit as Professeur d'echange. Finally we would like to thank W.G. Love for helpful discussions in the course of the microscopic calculations.

References

* On leave from University of Alberta, Edmonton Alberta, Canada.

1. G.F. Bertsch, Nucl. Phys. A354, 157 (1981).
2. A. Arima and H. Hyuga, in Mesons in Nuclei, edited by M. Rho and D.H. Wilkinson, (North-Holland, Amsterdam, 1979), Vol. II, p. 683.
3. W.G. Love, in The (p,n) Reaction and the Nucleon-Nucleon Force, edited by C.D. Goodman et al., (Plenum Press, New York, 1980), p. 23.
4. W.G. Love and M.A. Franey, Phys. Rev. C24, 1073 (1981).
5. S.-O. Bäckman and W. Weise, in Mesons in Nuclei, edited by M. Rho and D.H. Wilkinson, (North-Holland, Amsterdam, 1979), Vol. III, p. 1095.
6. H. Toki and W. Weise, Phys. Rev. Lett. 42, 1034 (1979).
7. G.E. Brown, J.S. Dehesa, and J. Speth, Nucl. Phys. A330, 290 (1979).
8. W. Knüpfer, R. Frey, A. Friebel, W. Mettner, D. Meuer, A. Richter, E. Spamer, and O. Titze, Phys. Lett. 77B, 367 (1978).
9. A. Richter, in Nuclear Physics with Electromagnetic Interactions, edited by H. Arenhovel and D. Drechsel, Lecture Notes in Physics, Vol. 108 (Springer, Berlin, 1979), p. 19.
10. F.E. Cecil, G.T. Garvey and W.J. Braithwaite, Nucl. Phys. A232, 22 (1974).

11. H. Ikegami, T. Yamazaki, S. Morinobu, I. Katayama, M. Fujiwara, Y. Fujita, T. Itahashi, and S.I. Hayakawa, in Proceedings of the Symposium on Highly Excited States in Nuclear Reactions, Osaka, edited by H. Ikegami and M. Muraoka (Osaka University, Osaka 1980).

12. D.E. Bainum, J. Rapaport, C.D. Goodman, D.J. Horen, C.C. Foster, M.B. Greenfield, and C.A. Goulding, Phys. Rev. Lett. 44, 1751 (1980).

13. B.D. Anderson, J.N. Knudson, P.C. Tandy, J.W. Watson, R. Madey, and C.C. Foster, Phys. Rev. Lett. 45, 699 (1980).

14. C. Gaarde, J. Rapaport, T.N. Taddeucci, C.D. Goodman, C.C. Foster, D.E. Bainum, C.A. Goulding, M.B. Greenfield, D.J. Horen, and E. Sugarbaker, Nucl. Phys. A369, 258 (1981).

15. R.R. Doering, A. Galonsky, D.M. Patterson and G.F. Bertsch, Phys. Rev. Lett. 35, 1691 (1975).

16. N. Anantaraman, G.M. Crawley, A. Galonsky, C. Djalali, N. Marty, M. Morlet, A. Willis, and J.-C. Jourdain, Phys. Rev. Lett. 46, 1318 (1981).

17. F.E. Bertrand, E.E. Gross, D.J. Horen, J.R. Wu, J. Tinsley, D.K. McDaniels, L.W. Swenson, and R. Liljestrand, Phys. Lett. 103B, 326 (1981).

18. C. Djalali, N. Marty, M. Morlet, A. Willis, J.-C. Jourdain, N. Anantaraman, G.M. Crawley, A. Galonsky, and P. Kitching, to be published.

19. H. Toki, D. Cha, and G. Bertsch, Phys. Rev. C24, 1371, (1981).

20. N. Anantaraman and B.H. Wildenthal, following paper.

21. D. Meuer, R. Frey, D.H.H. Hoffmann, A. Richter, E. Spamer, O. Titze, and W. Knupfer, Nucl. Phys. A349, 309 (1980).

22. A. Willis, M. Morlet, N. Marty, R. Frascaria, C. Djalali, V. Comparat, and P. Kitching, Nucl. Phys. A344, 137 (1980).

23. M. Morlet and A. Willis, Orsay Report IPNO-PhN-79-15, 1979 (unpublished).

24. C. Djalali, N. Marty, M. Morlet and A. Willis, Nucl. Phys. A380, 42 (1982).

25. J.-P. Didelez, private communication.

26. W. Steffen, H.-D. Graf, W. Gross, D. Meuer, A. Richter, E. Spamer, and O. Titze, Phys. Lett. 95B, 23 (1980).

27. P. Schwandt, private communication.

28. T.N. Taddeucci, J. Rapaport, D.E. Bainum, C.C. Foster, C.D. Goodman, C. Gaarde, J. Larsen, C.A. Goulding, D.J. Horen, T. Masterson, and E. Sugarbaker, preprint (1981).

29. Y.W. Lui, J.D. Bronson, C.M. Rozsa, D.H. Youngblood, P. Bogucki and U. Garg, Phys. Rev. C24, 884 (1981).

30. F.E. Bertrand, Nucl. Phys. A354, 129 (1981).

31. C. Djalali, N. Marty, M. Morlet, A. Willis, V. Comparat and R. Frascaria, Z. Phys. A298, 79 (1980).

32. A. Galonsky et al., to be published.

33. F.E. Cecil, W.L. Bendel, L.W. Fagg, and E.C. Jones, as cited by A. Galonsky, in The (p,n) Reaction and the Nucleon-Nucleon Force, edited by C.D. Goodman et al., (Plenum Press, New York, 1980), p. 191.

34. R. Schaeffer and J. Raynal (unpublished).

35. A. Nadasen, P. Schwandt, P.P. Singh, W.W. Jacobs, A.D. Bacher, P.T. Debevec, M.D. Kaitchuck, and J.T. Meek, Phys. Rev. C23, 1023 (1981).

36. C. Djalali and A. Willis, private communication.

37. F. Perey - ORNL, unpublished.

38. A. Willis, Thesis (1968) unpublished.

39. G. Bertsch, D. Cha and H. Toki, Phys.Rev. C24, 533 (1981).

Table I. Excitation energies and widths of resonance in Zr isotopes.

Nucleus	E_x(MeV)	FWHM (MeV)	Base Width (MeV)	E_x^{*a}(MeV)
^{90}Zr	8.9±0.2	1.5±0.2	3.3±0.3	8.3±0.3
^{92}Zr	8.8±0.2	1.4±0.2	3.2±0.3	8.5±0.3
^{94}Zr	8.7±0.2	1.4±0.2	3.2±0.3	8.8±0.3
^{96}Zr	8.6±0.2	1.2±0.2	3.6±0.3	---

[a] E_x^* is the excitation energy of the analogue state relative to the ground-state analogue, from ref. 32.

TABLE II. Optical-model parameters used in the distorted-wave analysis of the reaction Zr(p,p') at E_p = 201 MeV.

Set	V (MeV)	r_o (fm)	a_o (fm)	W_s (MeV)	r_w (fm)	a_w (fm)	V_{so} (fm)	r_{so} (fm)	a_{so} (fm)	W_{so} (MeV)	r'_{so} (fm)	a'_{so} (fm)	r_C (fm)
I	16.5	1.26	0.74	16.6	1.17	0.82	1.87	1.06	0.60	-2.36	1.04	0.62	1.25
II	15.31	1.28	0.72	13.26	1.26	0.66	2.00	1.10	0.56	-1.56	1.10	0.56	1.26

Table III. Cross sections measured and calculated for the ^{Zr}(p,p')^{Zr} reaction at E_p=201 MeV to the M1 state.

Nucleus	$\sigma_{exp}(4^o)$ mb/sr	$\sigma_{calc}(4^o)$ mb/sr	$N=\sigma_{exp}/\sigma_{calc}$ [a]
^{90}Zr	2.8±0.4	13.2[b]	0.26
		7.3[c]	0.41
^{92}Zr	2.5±0.4	13.0[b]	0.19
^{94}Zr	3.0±0.4	12.4[b]	0.26
^{96}Zr	3.0±0.4	No calculation	--

[a] N is obtained from the overall matching between the experimental and calculated angular distributions.

[b] DWBA70 calculation.

[c] RESEDA calculation.

Table IV: Comparison of (p,p') cross sections with predictions using (p,n) cross sections measured at 200 MeV.

	Simple wave functions mb/sr	Include mixing with low-lying states mb/sr	Include effect of iso-scalar terms mb/sr	Include Distortion effects mb/sr	Experimental mb/sr	$R=\frac{Experimental}{Predicted}$
Predicted (p,p') at 0^o from (p,n) at 0^o (50±12 mb/sr)	12.5	8.9	11.1	8.9	7.0	0.79
Predicted (p,p') at 4^o from (p,n) at 4^o (22±5.5 mb/sr)	5.5	3.9	4.9	3.9	2.8	0.72

Figure Captions

FIG. 1. Spectra of protons inelastically scattered from ^{40}Ca at 3^o and 7^o. Peaks due to oxygen contaminant are shown hatched.

FIG. 2. Spectra of protons inelastically scattered from ^{90}Zr, ^{92}Zr, ^{94}Zr and ^{96}Zr at 4^o. The arrows indicate the centroids of the M1 resonance.

FIG. 3. Spectra of protons inelastically scattered from ^{92}Zr at 3^o and 7^o.

FIG. 4. Angular distributions for the M1 state in ^{90}Zr, ^{92}Zr, ^{94}Zr and ^{96}Zr. The solid curves are DWBA70 calculations and the dashed curve is a RESEDA calculation (see section IV). All calculations are normalized to the data at forward angles. The dot-dashed curve is from a ^{90}Zr(p,n) measurement at 200 MeV (ref. 14).

FIG. 5. Elastic scattering angular distribution for ^{90}Zr (p,p) at 201 MeV. The dashed and solid curves are optical-model calculations using Set I and Set II optical potentials, respectively.

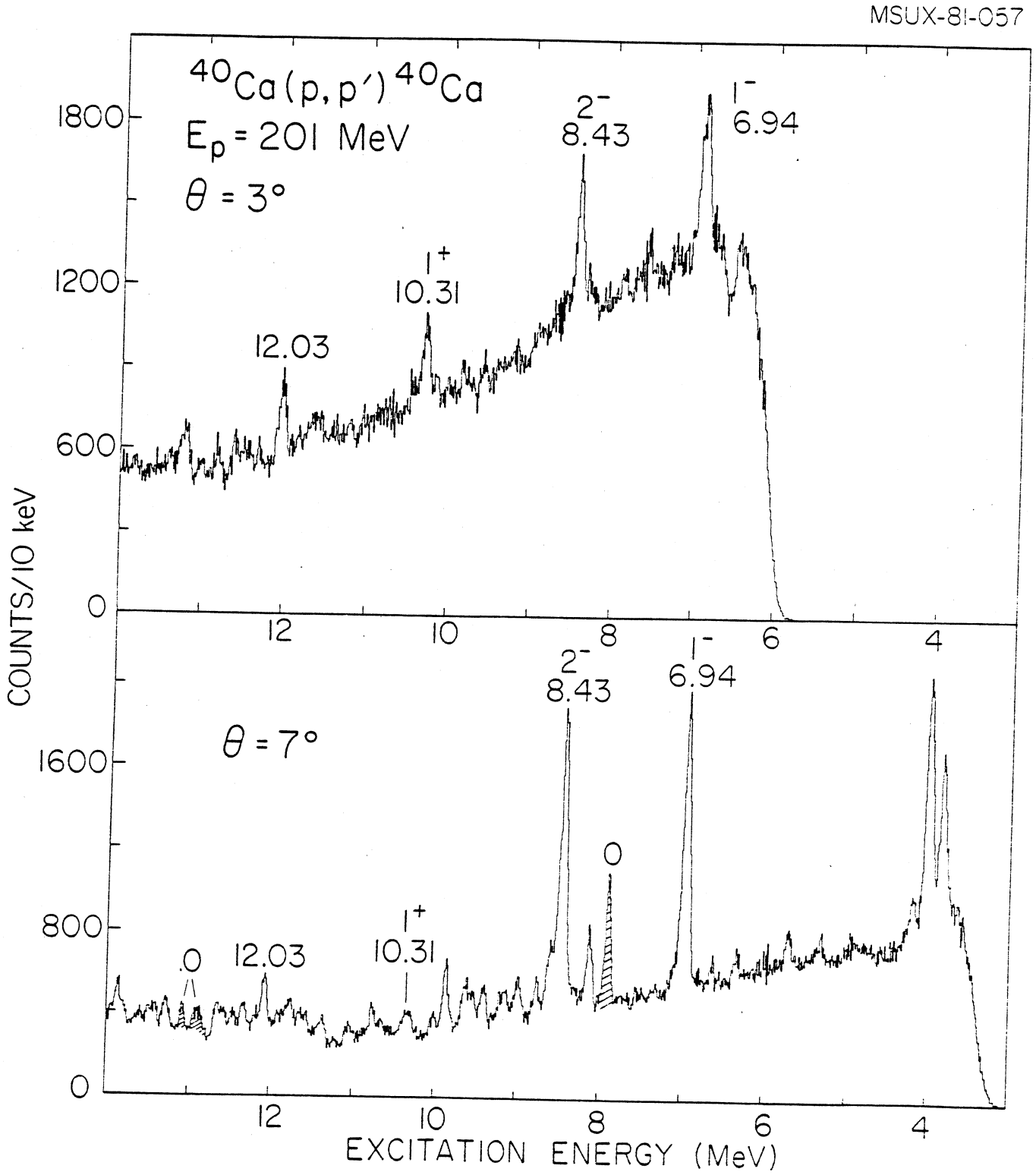
MSUX-81-057
$^{40}Ca(p,p')^{40}Ca$
E_p = 201 MeV
θ = 3°
2⁻ 8.43
1⁻ 6.94
1⁺ 10.31
12.03
1800
1200
600
0
θ = 7°
1600
800
0
0
12.03
1⁺ 10.31
2⁻ 8.43
0
1⁻ 6.94
12
10
8
6
4
COUNTS/10 keV
EXCITATION ENERGY (MeV)

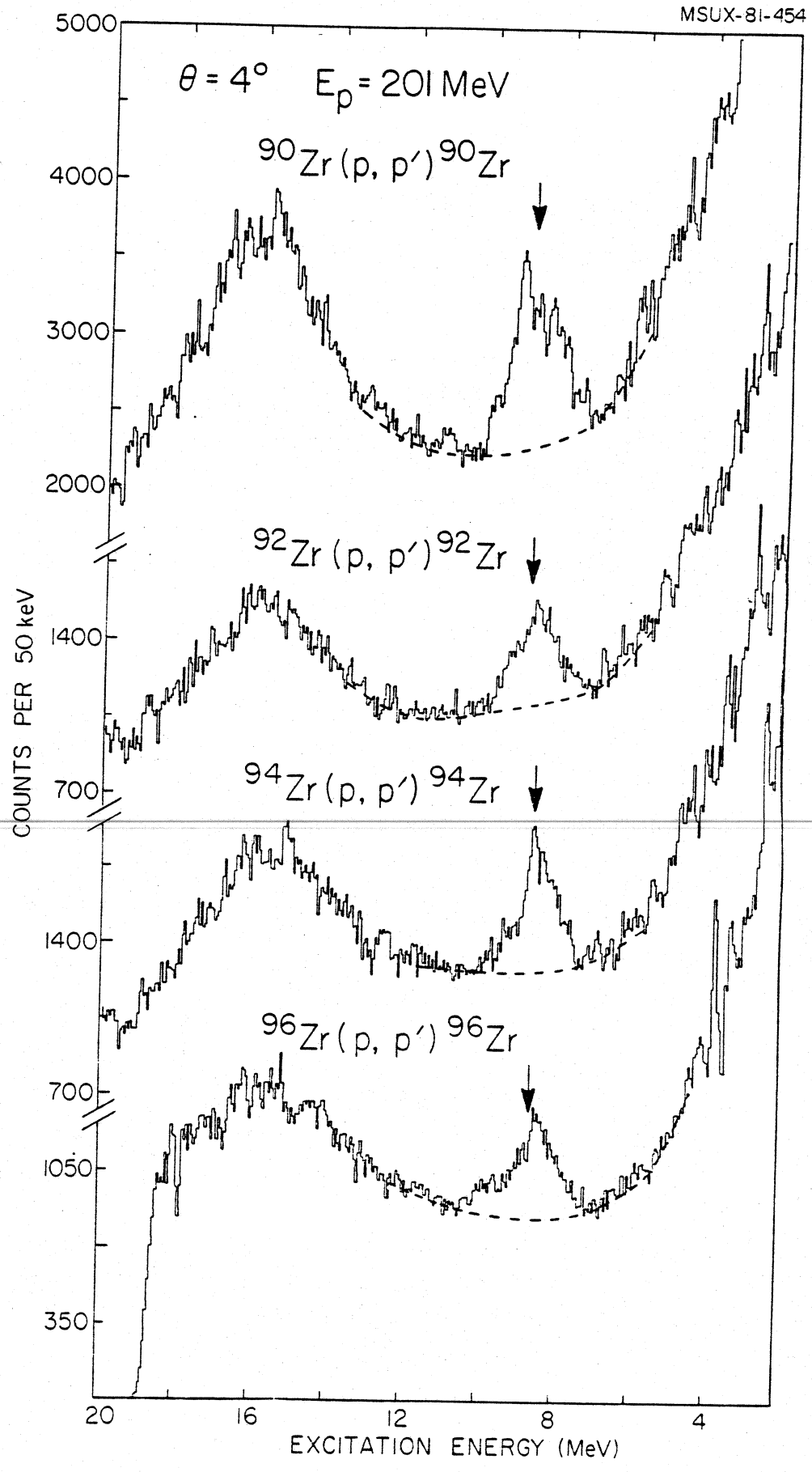
MSUX-81-454
θ = 4°
Ep = 201 MeV
90Zr (p, p′) 90Zr
92Zr (p, p′) 92Zr
94Zr (p, p′) 94Zr
96Zr (p, p′) 96Zr
COUNTS PER 50 keV
5000
4000
3000
2000
1400
700
1400
700
1050
350
20
16
12
8
4
EXCITATION ENERGY (MeV)

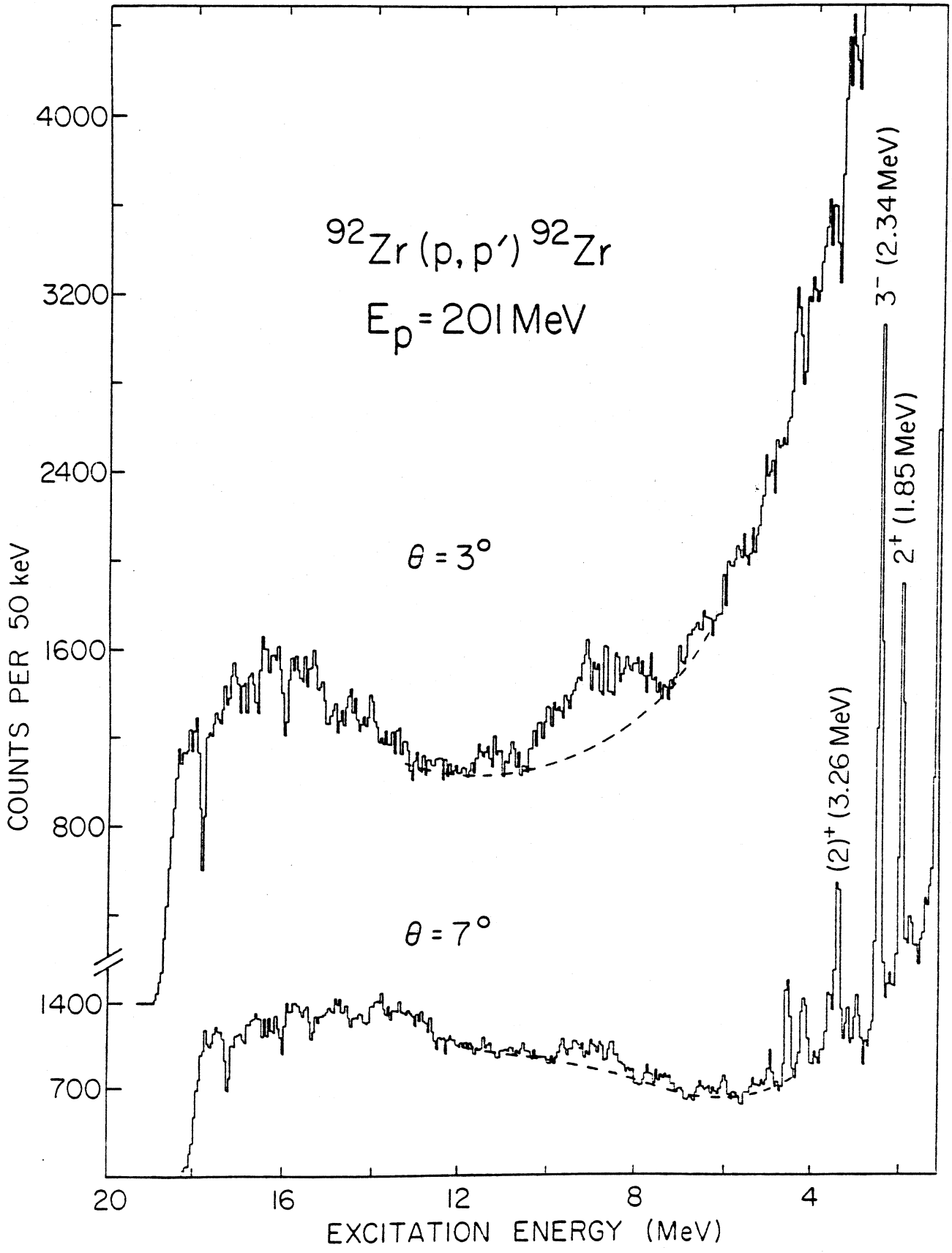
$^{92}Zr(p,p')^{92}Zr$
$E_p = 201$ MeV
$\theta = 3°$
$\theta = 7°$
3^- (2.34 MeV)
2^+ (1.85 MeV)
$(2)^+$ (3.26 MeV)
COUNTS PER 50 keV
4000
3200
2400
1600
800
1400
700
20
16
12
8
4
EXCITATION ENERGY (MeV)

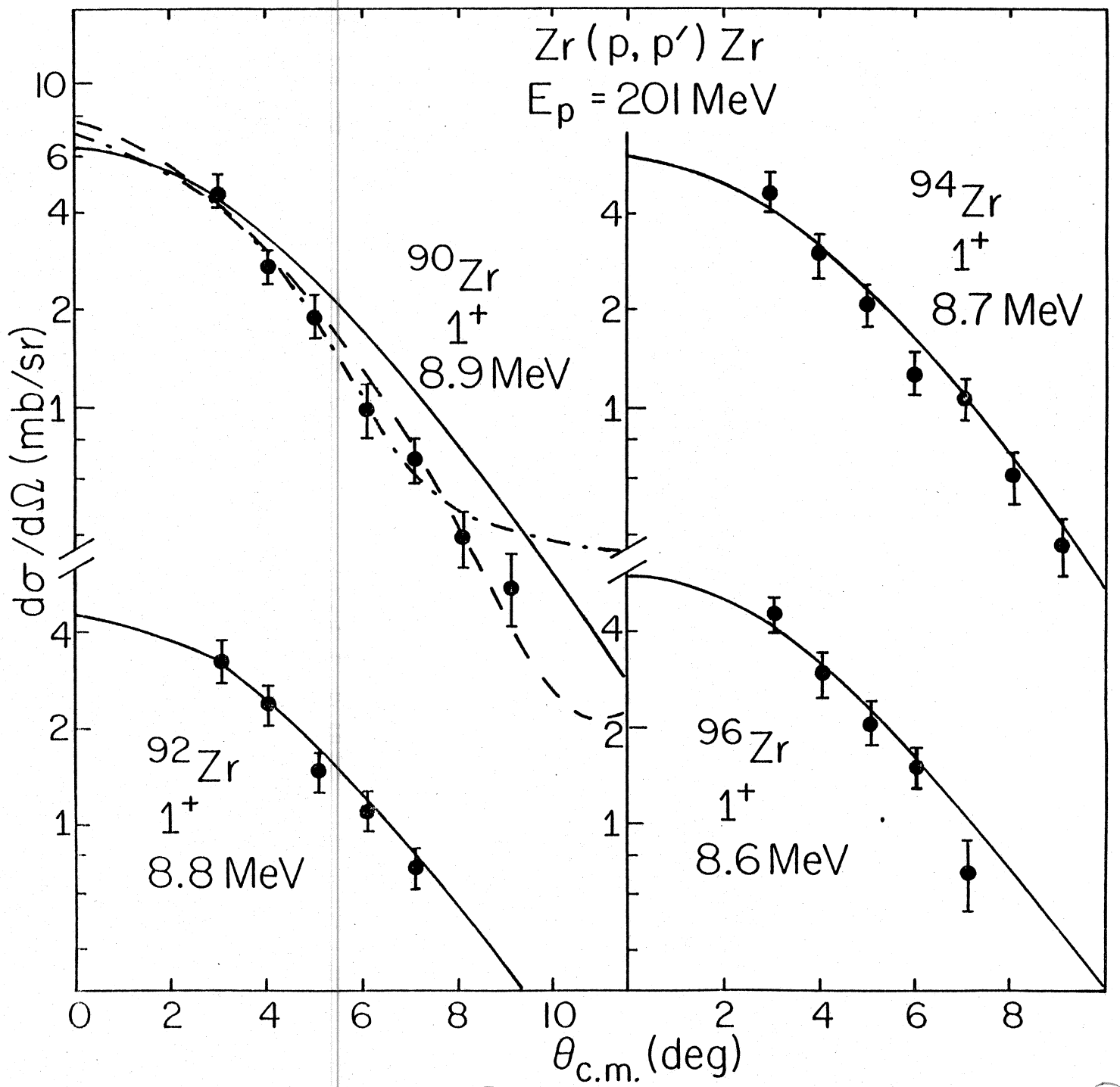
Zr (p, p′) Zr
Ep = 201 MeV
90Zr
1+
8.9 MeV
94Zr
1+
8.7 MeV
92Zr
1+
8.8 MeV
96Zr
1+
8.6 MeV
dσ/dΩ (mb/sr)
θc.m. (deg)

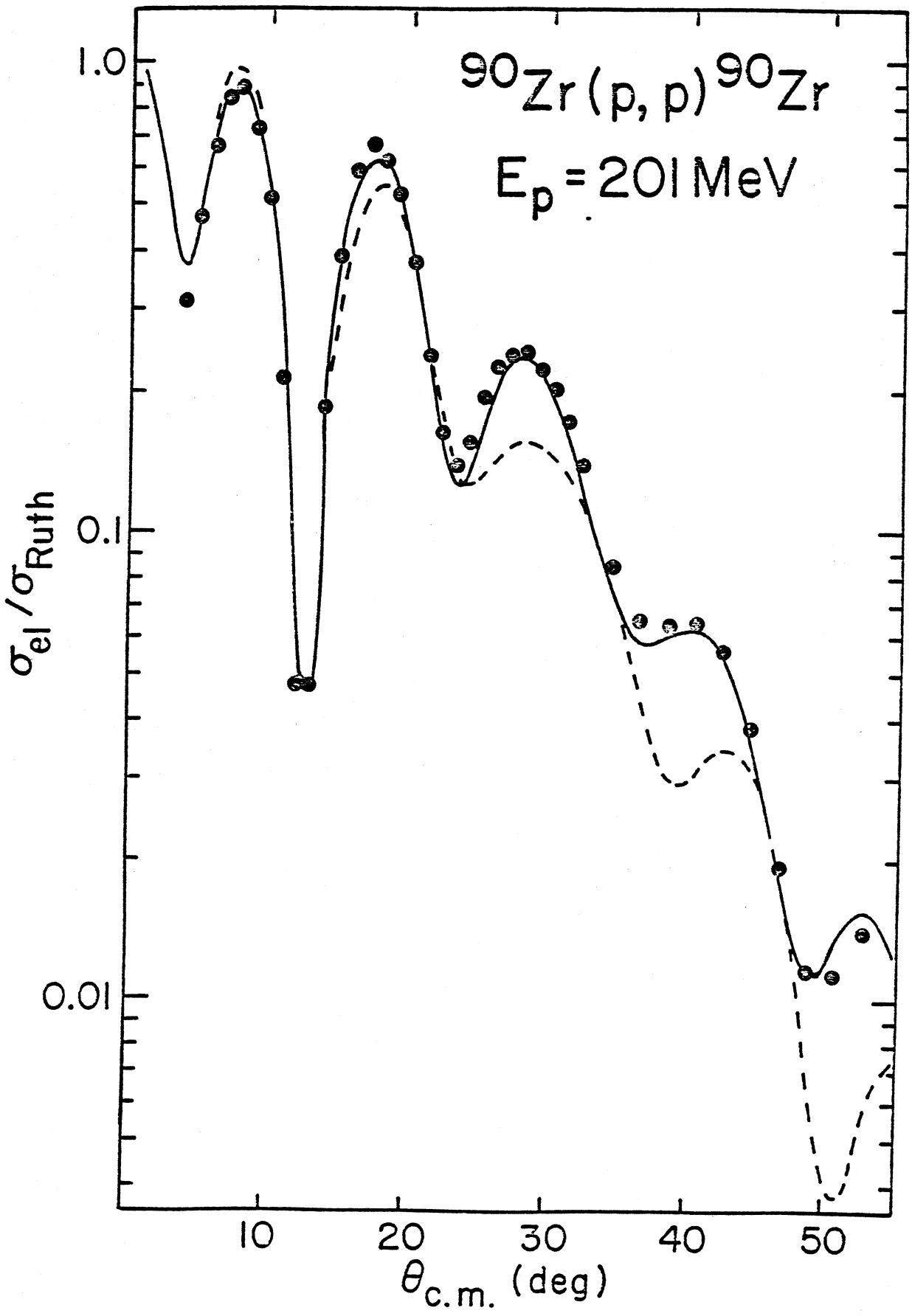
$^{90}Zr(p,p)^{90}Zr$
$E_p = 201$ MeV
1.0
0.1
0.01
$\sigma_{el}/\sigma_{Ruth}$
10
20
30
40
50
$\theta_{c.m.}$ (deg)